科学通报 2023 年 第 68 卷 第 5 期: 448 ~ 456
进 展
《中国科学》杂志社
SCIENCE CHINA PRESS

Pt合金催化剂电化学活性面积表征方法综述

张慧[1], 周芬[1,2], 潘牧[1,2*]

1. 武汉理工大学材料复合新技术国家重点实验室, 武汉 430070;
2. 先进能源科学与技术广东省实验室佛山仙湖实验室, 佛山 528200
* 联系人, E-mail: panmu@whut.edu.cn

2022-07-26 收稿, 2022-09-09 修回, 2022-09-19 接受, 2022-10-14 网络版发表
国家自然科学基金(21875177)资助

摘要 质子交换膜燃料电池(proton exchange membrane fuel cells, PEMFCs)作为高效清洁的电化学能源转换装置, 是目前应用最广泛、研究最热门的氢燃料电池之一. 基于PEMFCs的低成本与高性能需求, Pt合金催化剂极具研究前景. 电化学活性面积(electrochemical active surface area, ECSA)是筛选燃料电池高效催化剂以及研究催化动力学基础理论的重要参数, 其评价的准确性至关重要. 对于Pt/C催化剂ECSA的表征方法已经成熟, 然而Pt合金因其不同于Pt/C催化剂的化学组成和结构, 直接将传统Pt/C催化剂ECSA表征方法移植到Pt合金催化剂, 将不再满足表征准确性需求. 本文对Pt合金催化剂ECSA的表征方法及其表征ECSA偏差的来源进行综述.

关键词 质子交换膜燃料电池, Pt合金催化剂, 电化学活性面积, 物理表征, 电化学表征

质子交换膜燃料电池(proton exchange membrane fuel cells, PEMFCs)以其高效、环保等优势成为最重要的能量转换装置之一, 在过去的几十年, 丰田、现代、本田等汽车公司已初步实现质子交换膜燃料电池车的商业化[1,2]. 然而, 其进一步发展受PEMFCs成本和寿命限制[3,4]. Pt作为目前最高效的催化剂, 价格高昂, 其成本接近PEMFCs制造成本的一半[5,6]. 为了降低成本, Pt合金纳米催化剂成为主要研究方向之一. 通过非贵金属M(Ni、Co、Mn、Fe等)掺杂的方式制备PtM合金催化剂, 在降低铂含量的同时, 实现高催化活性和耐久性[7~9]. 以阴极催化剂为例, Pt合金催化剂的氧还原反应(oxygen reduction reaction, ORR)活性比Pt催化剂高近20倍, 因此在相同的电池性能需求下, 可大幅降低Pt用量[10]. 目前, PtCo合金催化剂已应用到2014年丰田推出的第一代Mirai燃料电池汽车, 开启PtCo合金催化剂的车载应用新纪元[11]. 此外, 据报道2021年丰田推出的第二代Mirai燃料电池汽车, 仍然是采用新型的PtCo合金催化剂, 并将面积比功率提升了15%, 单位功率Pt载量降低58%. 可见, Pt合金催化剂在PEMFCs未来的发展中是极有前景的.

电化学活性面积(electrochemical active surface area, ECSA)是指单位质量催化剂实际参与电化学催化反应的表面积. 一方面, 它不仅作为衡量催化剂活性位点数的指标, 同时在评价催化剂活性的其他指标中也充当重要参数. 例如, 面积比活性(specific activity, SA)和电荷转移阻抗(change transfer resistance, R_{ct})等催化剂活性指标, 均需要通过ECSA进行归一化处理, 最终作为催化剂性能评估的统一标准[12,13]. 面积比活性表达式为

$$\mathrm{SA} = \frac{i_k}{\mathrm{ECSA} \times M}, \tag{1}$$

式中, i_k表示动力学电流[12], M表示电极上负载Pt的质

引用格式: 张慧, 周芬, 潘牧. Pt合金催化剂电化学活性面积表征方法综述. 科学通报, 2023, 68: 448–456
Zhang H, Zhou F, Pan M. Review on electrochemical active surface area characterization methods of Pt alloy catalysts (in Chinese). Chin Sci Bull, 2023, 68: 448–456, doi: 10.1360/TB-2022-0795

量. 另一方面, ECSA也是催化剂基础理论研究的重要参数, 如经典的Butler-Volmer方程. 因此, 准确的ECSA对于筛选出性能更好的催化剂以及研究电催化动力学基础理论至关重要. Butler-Volmer方程为

$$j_0 = j_0^0 \alpha_c L_c \left(\frac{P_r}{P_r^0}\right)^{\gamma} \exp\left[-\frac{E_c}{RT}\left(1-\frac{T}{T_0}\right)\right], \quad (2)$$

式中, j_0表示交换电流密度, j_0^0表示参考交换电流密度, α_c表示ECSA[14], L_c表示催化剂载量, P_r表示阴极侧气体压力, P_r^0表示参考压力, γ表示ORR动力学级数, E_c表示ORR的活化能垒, R表示理想气体常数, T表示热力学温度, T_0表示参考温度.

催化剂ECSA表征方法主要分为物理法和电化学法: 物理法主要包括X射线衍射(X-ray diffractometry, XRD)和透射电子显微镜(transmission electron microscopy, TEM); 电化学法则主要包括氢的欠电位沉积(H-upd)、一氧化碳剥离(CO-stripping)以及金属欠电位沉积. 物理法表征是在催化剂非工作环境中进行的非原位测试方法[15]. 该方法假设颗粒表面均具有电催化活性, 并将得到的几何比表面积作为ECSA, 与真实的催化剂表面活性面积存在不可忽略的差别. 电化学法的研究则可追溯到20世纪80年代, 主要分为单电池原位测试和半电池(旋转圆盘)非原位测试[16]. 其中H-upd和CO-stripping等方法在Pt/C催化剂ECSA的表征应用中已经十分成熟, 并且具有较高的准确性. 然而Pt合金催化剂与Pt/C催化剂在物理结构(组成、粒径、形状等)和化学性能(催化活性位点、活性强度等)方面均有显著不同[17,18]. 目前用于Pt/C催化剂ECSA表征的电化学法几乎原封不动地应用于Pt合金催化剂, 导致Pt合金催化剂ECSA表征结果误差较大.

本文总结了传统ECSA的表征方法, 并分析了不同的方法在Pt合金ECSA表征中的不足之处.

1 催化剂ECSA表征原理与方法

1.1 XRD

XRD技术是通过分析催化剂的X射线衍射图谱, 获得物质的物相和晶体结构信息[19]. 通过分析不同晶面的衍射峰, 采用Scherrer公式计算出晶面尺寸:

$$D = \frac{K\lambda}{B\cos(\theta)}, \quad (3)$$

式中, D表示垂直于衍射面的晶面尺寸, K表示Scherrer常数, λ表示X射线波长(Cu Kα辐射源, λ为1.541 Å), B表示样品的衍射峰半宽度, θ表示布拉格衍射角. 假设催化剂颗粒均为标准的球体, 采用式(4), 利用粒子表面积与质量的比值得到催化剂的ECSA:

$$\mathrm{ECSA} = \frac{\sum_i 4\pi r_i^2}{\sum_i \rho_i \frac{4}{3}\pi r_i^3} \approx \frac{3}{\rho r}, \quad (4)$$

式中, r表示粒子半径, ρ表示粒子密度.

XRD技术采用Scherrer公式计算出粒径尺寸, 不能直接观察催化剂的整体形貌. 对Scherrer公式中的参数进行分析时, 获取衍射峰半宽度的人为因素对ECSA结果的影响远大于Scherrer常数和X射线波长的影响[20]. 此外, 采用XRD法是基于两个公式计算ECSA, 会导致误差累积. 因此, XRD很少直接用于催化剂的ECSA的表征.

1.2 TEM

TEM技术可观察催化剂的亚显微结构或超微结构, 通过采集不同区域高分辨率图像中催化剂颗粒尺寸信息, 计算平均粒径. 获取颗粒尺寸的数据越多, 平均粒径的结果越可靠[15]. 假设催化剂颗粒为球体, 利用式(4)求取ECSA.

通常, TEM观察到的纳米催化剂颗粒主要为非规则形态, 在采集颗粒粒径时也存在不可避免的人为操作因素, 对结果影响较大[21]. TEM和XRD方法中催化剂粒径计算的原理不同, 导致平均粒径相差较大, 计算出的ECSA也存在一定差异[22]. 由于TEM可以更直观地观察到粒径形貌, 且在分析粒径时, 采集尽量多的数据可以很大程度上降低人为误差, 因此相较于XRD, 在计算ECSA时更多地采用TEM的结果.

XRD和TEM方法得到的粒径都是平均值, 且认为几何面积均为电化学活性面积. 基于此, 计算的几何面积被认为是Pt催化剂理论上的ECSA, 通常被用来评估催化剂Pt利用率[23,24]. 因此, TEM和XRD的计算结果具有重要的参考意义.

1.3 H-upd

在循环伏安法中, 对于Pt/C催化剂, H在Pt表面的吸附特性满单层吸附, 即1个Pt原子表面吸附1个H原子, 如式(5)所示[25]:

$$Pt+H^{+}+e^{-}\rightarrow Pt-H \quad (5)$$

图1为多晶Pt的循环伏安(cyclic voltammetry, CV)曲线, 可以看到H在Pt表面吸脱附产生响应电流, 呈现出明显的特征峰.

由于H在Pt不同晶面的吸附能力不同, 在循环伏安曲线上呈现不同的特征峰, 如图1所示, 位于0.3 V左右的“强吸附H”特征峰归因于H在短程有序Pt(100)晶面上的吸附, 而位于0.1 V左右的“弱吸附H”特征峰则归结于H在Pt(110)台阶位点或短程有序Pt(111)晶面上的吸附[26~28]. 最终通过3个低指数晶面(111)、(110)和(100)的表面原子密度平均值获得计算ECSA的经验常数2.1 C m^{-2}. 利用H吸/脱附(特征峰积分面积)产生的电量可计算ECSA:

$$ECSA=\frac{S}{2.1\times\upsilon\times M}, \quad (6)$$

式中, S表示H在Pt表面吸附或脱附产生的电流响应对应于CV曲线中电流与电压的积分面积或吸脱附面积的平均值, 该面积($A\times V$)需要利用双电层对H的吸附或是脱附区进行背景扣除[28]; 2.1表示H在Pt表面的电荷密度(C m^{-2}), υ表示扫描速率(V s^{-1}), M表示电极上负载Pt的质量(g).

1.4 CO-stripping测试方法

CO-stripping与H-upd的测试方法在计算ECSA的原理时类似. CO在0.2 V恒电位下在Pt表面吸附, 再进行CV测试, 吸附的CO在高电位下氧化为CO_2, 该过程使CO从Pt表面剥离, 反应产生的电量在高电位形成1个或多个氧化峰[29]. 图2为常见多晶Pt的CO-stripping伏安图[30].

与H-upd不同的是, H对应1个电子的转移, 而CO通常对应2个电子的转移, 如式(7)和(8)所示, 而ECSA可通过式(9)计算[31]:

$$H_2O+Pt\rightarrow Pt-OH_{ads}+H^{+}+e^{-} \quad (7)$$

$$Pt-CO_{ads}+Pt-OH_{ads}\rightarrow CO_2+H^{+}+e^{-}+2Pt \quad (8)$$

$$ECSA=\frac{S}{4.2\times\upsilon\times M}, \quad (9)$$

式中, S表示CO在Pt表面氧化产生电流响应的峰面积[32]; 4.2表示单位面积Pt上的CO解吸电荷量(C m^{-2}).

1.5 金属欠电位沉积

金属欠电位沉积是指对于某种金属, 在比其热力学可逆电位更正的附加电位下, 可在其他基体上沉积的电化学现象, 其中沉积金属的功函数要小于基体材料的功函数[33]. 沉积金属在基体上剥离时形成的溶出产生的电荷经过双电层电容与H脱附电量进行修正, 与CO-stripping类似, 再根据峰面积计算ECSA, 如式(9)所示. 但不同的沉积金属对应的参数4.2 C m^{-2}需要校正[34,35]. 其中常见的沉积金属如Cu、Ag和Pb在Pt表面进行剥离时的电荷密度分别为4.2、2.1和3 C m^{-2}[31,36]. 以Cu为例, 假设每个Cu能转移两个电子, Cu能在Pt表面形成近乎封闭的Cu单层[37]:

$$Cu_{upd}\rightarrow Cu^{2+}+2e^{-} \quad (10)$$

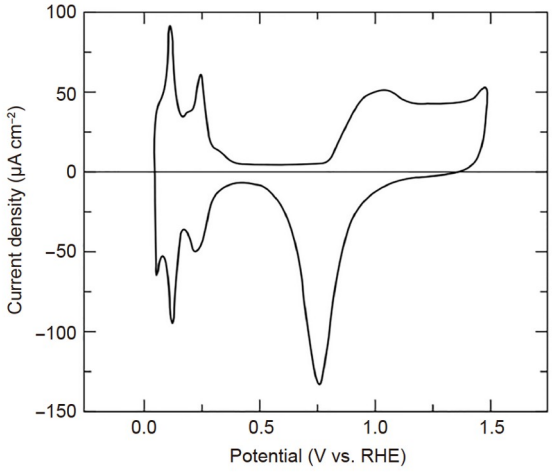

图 1 氮气氛围0.5 mol L^{-1} H_2SO_4溶液中的多晶Pt的CV图, 扫描速率50 mV s^{-1}[25]

Figure 1 Cyclic voltammogram of polycrystalline Pt in 0.5 mol L^{-1} H_2SO_4 solution in nitrogen atmosphere, with a scan rate of 50 mV s^{-1}[25]

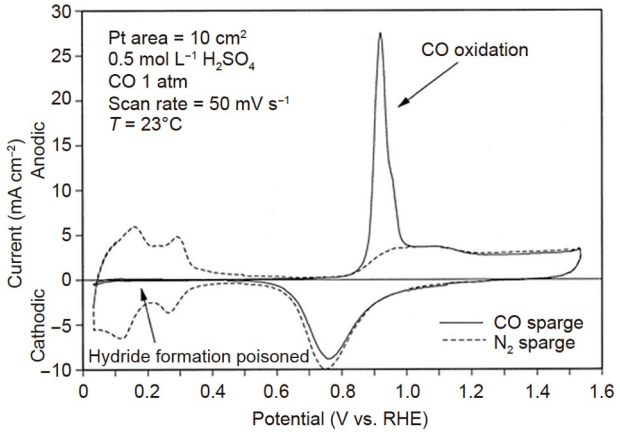

图 2 23°C下, 多晶Pt的CO-stripping伏安图[30]

Figure 2 CO-stripping voltammogram of polycrystalline Pt at 23°C[30]

2 Pt合金ECSA表征方法的工作评述

基于XRD和TEM表征ECSA的原理, 这类方法可以直接用于Pt合金ECSA表征, 但也存在与Pt催化剂同样的表征不准确问题. 本节主要分析电化学方法H-upd、CO-stripping和金属欠电位沉积表征Pt合金催化剂ECSA的局限性及偏差来源.

2.1 H-upd的偏差来源

采用H-upd表征ECSA时, Pt合金催化剂Pt表面H的吸脱附特征峰变得模糊[13,38]. 这与Pt合金的组成、粒径大小, 形态结构发生的变化而导致的配体、应变以及电子效应息息相关[26,39]. PtCo/C催化剂的CV特征曲线如图3所示[40]. Pt合金与纯Pt的结构差别不仅会影响ECSA计算式(6)中分母中的经验常数2.1 C m^{-2}, 同时会影响分子代表的H吸/脱附积分面积的大小.

当与Pt合金化的金属为非贵金属时, 如Fe、Co、Ni等, 在酸性条件下, 合金中的非贵金属极易溶解, 导致合金表面产生富Pt(Pt-skin)结构或Pt骨架(Pt-skeleton)结构[41,42]. 合金表面虽依旧为Pt, 但次表层以及内部的合金成分导致H在Pt表面的覆盖率降低. 相对于Pt/C表面H的吸脱附电荷密度为2.1 C m^{-2}, Pt-skin结构仅有1.8 C m^{-2}, 而Pt-skeleton结构也降低到2 C m^{-2}, 因此在计算此类合金催化剂的ECSA时, 若直接采用Pt/C表面H的吸脱附电荷密度, 得到的ECSA将被低估[43]. 在Ni或Co等非贵金属原子占比不同的碳负载Pt合金催化剂中, CV曲线会呈现不同的H吸脱附面积[44]. 如图4所示, 当第二金属Ni或Co在Pt合金中含量增加时, H吸脱附面积不断变小, 同时表面电化学行为的变化也导致单位Pt表面吸脱附电荷密度的变小[45]. Becknell等人[46]表明根据合金化结构的不同, 其真实ECSA可被低估约1.5倍.

当Pt催化剂中掺入化学性质稳定的铂族金属时, Pt族金属基本不会在酸性活化过程中溶解, 仍存在于催化剂颗粒表面. H在贵金属Rh、Ir或Pd表面的电荷密度经验值分别为2.21、2.18或2.05 C m^{-2}, 与Pt合金化后, 参与表面H的吸脱附, 则需要重新考量ECSA计算公式中的2.1 C m^{-2}[47~49]. Czerwinski和Sobkowski[50]假设PtRh的吸附能力在Pt与Rh之间, 且H在合金表面的电荷密度与Pt、Rh的组分呈线性关系, 因此在ECSA的公式中引入了合金组分中不同原子比率参数. 另外, 对于PtRu合金, H的吸附区与O吸附区重叠, 并且Ru会将部分吸附H储存在次表层中, 对实际积分面积造成干扰, 因此一般不会采用H-upd来衡量PtRu合金催化剂ECSA[51].

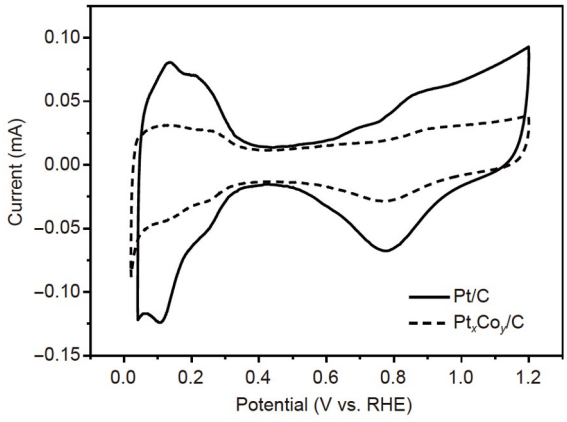

图 3 氮气氛围0.1 mol L^{-1} $HClO_4$ 溶液中Pt/C(实线)和Pt_xCo_y/C(虚线)催化剂的循环伏安图, 扫描速率为20 mV s^{-1}[40]

Figure 3 Cyclic voltammogram of Pt/C (solid line) and Pt_xCo_y/C (dotted line) catalysts in 0.1 mol L^{-1} $HClO_4$ solution in nitrogen atmosphere with a scan rate of 20 mV s^{-1}[40]

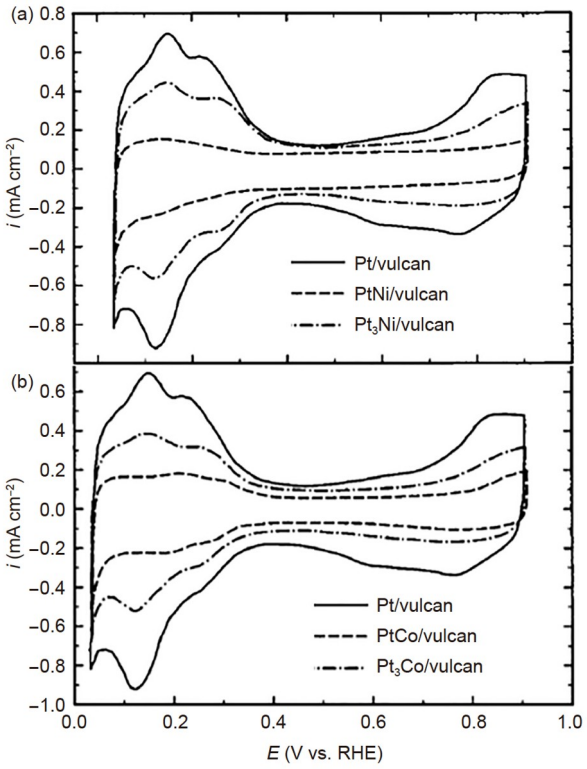

图 4 氩气饱和下的0.1 mol L^{-1} $HClO_4$溶液中负载型Pt催化剂与负载型Pt_3Ni和PtNi催化剂(a)和负载型Pt催化剂与负载型Pt_3Co和PtCo催化剂(b)的循环伏安图, 扫描速率50 mV s^{-1}[45]

Figure 4 Cyclic voltammograms of supported Pt catalysts and supported Pt_3Ni and PtNi catalysts (a), and supported Pt catalysts and supported Pt_3Co and PtCo catalysts (b) in 0.1 mol L^{-1} $HClO_4$ solution in argon saturation, with a sweep rate of 50 mV s^{-1}[45]

采用H-upd评估Pt合金的ECSA时，从ECSA计算公式上看，无论由于合金化后表面吸附能力还是单位面积吸附电荷量的变化都将导致Pt合金催化剂的ECSA表征结果出现较大偏差.

2.2 CO剥离的偏差来源

CO在Pt表面吸附量也受不同晶面原子密度的影响[52]. Pt与非贵金属形成合金催化剂时，催化剂次表层将极大影响CO在其表面的吸附能力[53]. 即使Pt/C或Pt合金催化剂具有基本相同的几何表面积、表面成分和表面结构，两者对CO的电化学吸附能力却大不相同. Stamenkovi研究团队[54]采用旋转圆盘电极(rotating disk electrode，RDE)进行CO-stripping测试时发现，Pt_3Ni(111)/C的CO氧化峰明显向低电位偏移且峰高变小，积分面积发生变化(图5)，这归因于次表层的Ni影响了Pt表面CO的氧化过程. 单位面积Pt_3Ni(111)和Pt_3Co(111)上的CO解吸电荷量变小，分别为3.04和2.83 C m^{-2}，远小于Pt/C催化剂的4.2 C m^{-2}，最终造成了ECSA的低估[54].

当化学性质稳定的贵金属作为Pt合金化的金属时，催化剂表面的合金金属不仅与Pt一起参与CO的电吸附，同时内层的合金金属也会影响表面的CO吸附[55]. 相对于H-upd过程1个电子转移的吸脱附行为，CO-stripping更为复杂，CO在Pt、Rh、Pd等金属上存在不同形式的吸附. 最常见的有线式吸附(CO与每个金属位点的比例为1:1)和桥式吸附(CO与每个金属位点的比例为2:1)[56]，最终会体现在CO解吸电荷量上，如Rh为4.4 C m^{-2}[57]. 其他金属掺入产生的不同吸附方式导致CO在Pt表面的吸附不是一一对应的，即吸附形式改变了转移电荷量. 通过原位红外光谱技术发现，不同的金属团簇存在不同的CO吸附方式，则不能使用单一CO解吸电荷量来计算ECSA[58]. Ru金属表面吸附的CO氧化峰值电位约在0.55 V，与Pt的CO氧化峰几乎没有重叠，但PtRu合金化后，CO氧化峰向更低的电位偏移，此时采用4.2 C m^{-2}得到的表面积存在倍数级偏差[59].

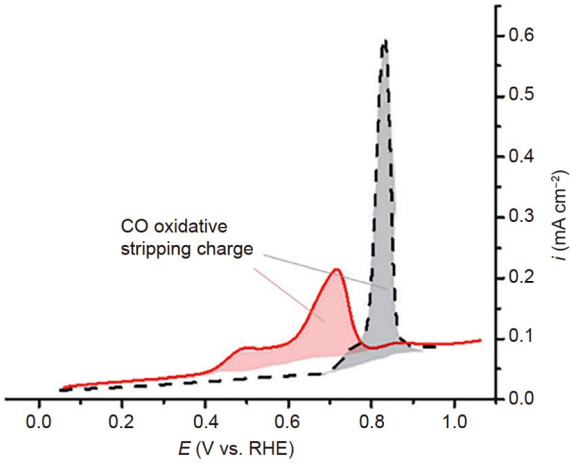

图 5 (网络版彩色)0.1 mol L^{-1} $HClO_4$溶液中Pt/C(黑线)和PtNi/C-skin(红线)的CO-stripping曲线[54]

Figure 5 (Color online) CO-stripping curves of Pt/C (black line) and PtNi/C-skin (red line) in 0.1 mol L^{-1} $HClO_4$ solution[54]

CO-stripping与H-upd原理类似，都是通过不同物质在Pt表面进行吸脱附产生的峰面积计算ECSA[60]. 同样，H在Pt合金表面的吸附性质变化趋势也发生在CO吸附于Pt合金表面上. Garrick等人[61]在单电池中对Pt-Co/C和Pt-Ni/C催化剂进行H-upd和CO-stripping测试，均发现$ECSA_{H\text{-}upd} < ECSA_{CO\text{-}stripping}$. 采用电化学方法时，即使Pt合金表面的吸附性能变弱，但Pt合金表面对CO的吸附能力仍强于H. 因而与H-upd相比，采用CO-stripping能获得较为准确的Pt合金催化剂的ECSA.

2.3 金属欠电位沉积的偏差来源

当贵金属为合金金属时，沉积金属在Pt合金表面形成完整的单层前可能已经开始多层沉积，即沉积金属原子与被沉积基体表面原子比不能满足1:1的对应关系，将同时影响沉积金属剥离时的积分面积和单位面积剥离电荷量[62]. 此外，在PtPd合金表面进行Cu-upd时发现，PtPd表面的Cu吸附峰可能会与氧的吸附峰重叠，是ECSA评估偏差的主要来源[63]. 当非贵金属为合金金属时，Cu在Pt合金表面的吸附能力会减弱，Shao等人[64]对PtNi/C采用Cu-upd的测试方法发现，Cu只能在该合金表面形成93%单层的覆盖率，尽管可以通过调整扫描速率来提高Cu单层的覆盖率，但ECSA的计算仍存在偏差. 并且，金属欠电位沉积的使用需要在含有适当金属盐的电解质溶液，不能应用在单电池测试中，即对于原位测试ECSA结果的准确性不明确[65].

在实际催化反应过程中，合金催化剂中不同金属对催化活性的贡献是不同的. 以PtRu为例，Cu在两者上均有沉积，并且两种金属各自的面积可通过Cu剥离峰定量[59]. Ru具有氧还原催化活性，但贡献弱于Pt[66]. 若将两种金属的剥离峰面积简单相加，会高估其ECSA；若仅以Pt表面的剥离峰积分获取ECSA，则忽略了Ru对氧还原的贡献，将会低估其ECSA. 因此，在准确评估ECSA时，还应考虑合金金属对催化活性的贡献程度.

3 总结与展望

Pt合金催化剂表面特性受多方面因素的影响, 目前并没有一个普适性的方法用于准确表征其ECSA. 由于催化剂颗粒自身的形状与表面活性位点的差异, XRD与TEM表征合金催化剂ECSA的结果与电化学表征结果产生的偏差远大于Pt/C催化剂. Pt合金催化剂表面吸附能力的改变表明, 在测试ECSA时, 适用于Pt/C的H和CO等探针物质并不能直接用于Pt合金上. 直接采用H-upd和CO-stripping等电化学法通常会低估Pt合金催化剂的活性面积, 而导致在与Pt/C催化剂进行比较时, 夸大了Pt合金催化剂的比活性. 为更客观地评价Pt合金催化剂的性能, 深入了解不同Pt合金的表面结构与吸附能及吸附物种的覆盖率关系, 修正ECSA的计算公式, 或创新地开发新电化学法来准确表征Pt合金的ECSA, 对开发新型高性能Pt合金催化剂及其在PEMFCs中的商业应用具有重要的研究意义.

参考文献

1 Wang Y, Diaz D F R, Chen K S, et al. Materials, technological status, and fundamentals of PEM fuel cells—A review. Mater Today, 2020, 32: 178–203

2 Pollet B G, Kocha S S, Staffell I. Current status of automotive fuel cells for sustainable transport. Curr Opin Electrochem, 2019, 16: 90–95

3 Moreno N G, Molina M C, Gervasio D, et al. Approaches to polymer electrolyte membrane fuel cells (PEMFCs) and their cost. Renew Sustain Energy Rev, 2015, 52: 897–906

4 Zhao L T, Cheng X J, Luo L X, et al. Progress and prospects of low platinum oxygen reduction catalysts for proton exchange membrane fuel cells (in Chinese). Chin Sci Bull, 2022, 67: 2212–2225 [赵路甜, 程晓静, 罗柳轩, 等. 低铂质子交换膜燃料电池氧还原催化剂的研究进展与展望. 科学通报, 2022, 67: 2212–2225]

5 Zhang S, Yuan X Z, Hin J N C, et al. A review of platinum-based catalyst layer degradation in proton exchange membrane fuel cells. J Power Sources, 2009, 194: 588–600

6 Wang J, Ding W, Wei Z D. Performance of polymer electrolyte membrane fuel cells at ultra-low platinum loadings (in Chinese). Acta Phys Chim Sin, 2021, 37: 2009094 [王建, 丁炜, 魏子栋. 超低铂用量质子交换膜燃料电池. 物理化学学报, 2021, 37: 2009094]

7 Banham D, Ye S. Current status and future development of catalyst materials and catalyst layers for proton exchange membrane fuel cells: An industrial perspective. ACS Energy Lett, 2017, 2: 629–638

8 Brouzgou A, Seretis A, Song S, et al. CO tolerance and durability study of PtMe (Me = Ir or Pd) electrocatalysts for H_2-PEMFC application. Int J Hydrog Energy, 2021, 46: 13865–13877

9 Li J, Feng X, Wei Z D. Recent progress in Pt-based catalysts for oxygen reduction reaction (in Chinese). J Electrochem, 2018, 24: 589–601 [李静, 冯欣, 魏子栋. 铂基燃料电池氧还原反应催化剂研究进展. 电化学, 2018, 24: 589–601]

10 van der Vliet D F, Wang C, Tripkovic D, et al. Mesostructured thin films as electrocatalysts with tunable composition and surface morphology. Nat Mater, 2012, 11: 1051–1058

11 Yoshida T, Kojima K. Toyota mirai fuel cell vehicle and progress toward a future hydrogen society. Interface Mag, 2015, 24: 45–49

12 Li W, Haldar P. Highly active carbon supported core-shell PtNi@Pt nanoparticles for oxygen reduction reaction. Electrochem Solid-State Lett, 2010, 13: B47

13 Rao Y, Cai C, Tan J, et al. Oxygen reduction activity indicator for fuel cell catalysts at rated voltage. J Electrochem Soc, 2019, 166: F351–F356

14 Zhang J, Wu J, Zhang H, et al. PEM Fuel Cell Testing and Diagnosis. Amsterdam: Elsevier, 2013

15 Schulenburg H, Durst J, Müller E, et al. Real surface area measurements of Pt_3Co/C catalysts. J Electroanal Chem, 2010, 642: 52–60

16 Furuya N, Koide S. Hydrogen adsorption on platinum single-crystal surfaces. Surf Sci, 1989, 220: 18–28

17 Campos-Roldán C A, Pailloux F, Blanchard P Y, et al. Rational design of carbon-supported platinum-gadolinium nanoalloys for oxygen reduction reaction. ACS Catal, 2021, 11: 13519–13529

18 Humbert M, Chen J. Correlating hydrogenation activity with binding energies of hydrogen and cyclohexene on M/Pt(111) (M = Fe, Co, Ni, Cu) bimetallic surfaces. J Catal, 2008, 257: 297–306

19 Christmann K, Friedrich K A, Zamel N. Activation mechanisms in the catalyst coated membrane of PEM fuel cells. Prog Energy Combust Sci, 2021, 85: 116140

20 Paulus U A, Wokaun A, Scherer G G, et al. Oxygen reduction on high surface area Pt-based alloy catalysts in comparison to well defined smooth bulk alloy electrodes. Electrochim Acta, 2002, 47: 3787–3798

21 Zalitis C, Kucernak A, Lin X, et al. Electrochemical measurement of intrinsic oxygen reduction reaction activity at high current densities as a function of particle size for $Pt_{4-x}Co_x$/C (x = 0, 1, 3) catalysts. ACS Catal, 2020, 10: 4361–4376

22 Li B, Yan Z, Xiao Q, et al. Highly active carbon-supported Pt nanoparticles modified and dealloyed with Co for the oxygen reduction reaction. J Power Sources, 2014, 270: 201–207

23 Bhuvanendran N, Ravichandran S, Xu Q, et al. A quick guide to the assessment of key electrochemical performance indicators for the oxygen reduction reaction: A comprehensive review. Int J Hydrog Energy, 2022, 47: 7113–7138

24 Uchida M, Park Y C, Kakinuma K, et al. Effect of the state of distribution of supported Pt nanoparticles on effective Pt utilization in polymer electrolyte fuel cells. Phys Chem Chem Phys, 2013, 15: 11236–11247

25 Vielstich W. Cyclic Voltammetry. Handbook of Fuel Cells. New York: Wiley, 2010

26 Trasatti S, Petrii O A. Real surface area measurements in electrochemistry. J Electroanal Chem, 1992, 327: 353–376

27 Hayes M, Kuhn A T. Determination of platinum catalyst surface area with potentiodynamic techniques—Effect of experimental parameters. Appl Surf Sci, 1980, 6: 1–14

28 Carter R N, Kocha S S, Wagner F, et al. Artifacts in measuring electrode catalyst area of fuel cells through cyclic voltammetry. ECS Trans, 2007, 11: 403–410

29 Ciapina E G, Santos S F, Gonzalez E R. Electrochemical CO stripping on nanosized Pt surfaces in acid media: A review on the issue of peak multiplicity. J Electroanal Chem, 2018, 815: 47–60

30 Bellows R J, Marucchi-Soos E P, Buckley D T. Analysis of reaction kinetics for carbon monoxide and carbon dioxide on polycrystalline platinum relative to fuel cell operation. Ind Eng Chem Res, 1996, 35: 1235–1242

31 Vidaković T, Christov M, Sundmacher K. The use of CO stripping for *in situ* fuel cell catalyst characterization. Electrochim Acta, 2007, 52: 5606–5613

32 Schmidt T J, Gasteiger H A, Stäb G D, et al. Characterization of high-surface-area electrocatalysts using a rotating disk electrode configuration. J Electrochem Soc, 1998, 145: 2354–2358

33 Shao M, Chang Q, Dodelet J P, et al. Recent advances in electrocatalysts for oxygen reduction reaction. Chem Rev, 2016, 116: 3594–3657

34 Sudha V, Sangaranarayanan M V. Underpotential deposition of metals—Progress and prospects in modelling. J Chem Sci, 2005, 117: 207–218

35 Sudha V, Sangaranarayanan M V. Underpotential deposition of metals: Structural and thermodynamic considerations. J Phys Chem B, 2002, 106: 2699–2707

36 Liu Y, Bliznakov S, Dimitrov N. Comprehensive study of the application of a Pb underpotential deposition-assisted method for surface area measurement of metallic nanoporous materials. J Phys Chem C, 2009, 113: 12362–12372

37 Varga K, Zelenay P, Wieckowski A. Adsorption of anions on ultra-thin metal deposits on single-crystal electrodes. J Electroanal Chem, 1992, 330: 453–467

38 Escudero-Escribano M, Verdaguer-Casadevall A, Malacrida P, et al. Pt_5Gd as a highly active and stable catalyst for oxygen electroreduction. J Am Chem Soc, 2012, 134: 16476–16479

39 Voiry D, Chhowalla M, Gogotsi Y, et al. Best practices for reporting electrocatalytic performance of nanomaterials. ACS Nano, 2018, 12: 9635–9638

40 Rao Y. Oxygen reduction activity indicator for fuel cell catalysts (in Chinese). Master Thesis. Wuhan: Wuhan University of Technology, 2019 [饶妍. 燃料电池额定电势下氧还原催化剂活性指示符研究. 硕士学位论文. 武汉: 武汉理工大学, 2019]

41 Kang Y S, Choi D, Park H Y, et al. Tuning the surface structure of PtCo nanocatalysts with high activity and stability toward oxygen reduction. J Industrial Eng Chem, 2019, 78: 448–454

42 Chen S, Ferreira P J, Sheng W, et al. Enhanced activity for oxygen reduction reaction on "Pt_3Co" nanoparticles: Direct evidence of percolated and sandwich-segregation structures. J Am Chem Soc, 2008, 130: 13818–13819

43 Stamenkovic V R, Mun B S, Mayrhofer K J J, et al. Effect of surface composition on electronic structure, stability, and electrocatalytic properties of Pt-transition metal alloys: Pt-skin versus Pt-skeleton surfaces. J Am Chem Soc, 2006, 128: 8813–8819

44 Wakisaka M, Hyuga Y, Abe K, et al. Facile preparation and electrochemical behavior of $Pt_{100-x}Co_x$(111) single-crystal electrodes in 0.1 M $HClO_4$. Electrochem Commun, 2011, 13: 317–320

45 Paulus U A, Wokaun A, Scherer G G, et al. Oxygen reduction on carbon-supported Pt-Ni and Pt-Co alloy catalysts. J Phys Chem B, 2002, 106: 4181–4191

46 Becknell N, Kang Y, Chen C, et al. Atomic structure of Pt_3Ni nanoframe electrocatalysts by *in situ* X-ray absorption spectroscopy. J Am Chem Soc, 2015, 137: 15817–15824

47 Rand D A J, Woods R. The nature of adsorbed oxygen on rhodium, palladium and gold electrodes. J Electroanal Chem Interfacial Electrochem, 1971, 31: 29–38

48 Woods R. Hydrogen adsorption on platinum, iridium and rhodium electrodes at reduced temperatures and the determination of real surface area. J Electroanal Chem Interfacial Electrochem, 1974, 49: 217–226

49 Hara M, Linke U, Wandlowski T. Preparation and electrochemical characterization of palladium single crystal electrodes in 0.1 M H_2SO_4 and

$HClO_4$. Electrochim Acta, 2007, 52: 5733–5748
50 Czerwinski A, Sobkowski J. Electrosorption of CO and CO_2 on Pt-Rh alloy electrodes. Anal Lett, 1984, 17: 2175–2181
51 Vielstich W, Lamm A, Gasteiger H. Handbook of Fuel Cells: Fundamentals, Technology, Applications. Chichester: John Wiley and Sons, 2003
52 Inkaew P, Zhou W, Korzeniewski C. CO monolayer oxidation at Pt(100) probed by potential step measurements in comparison to Pt(111) and Pt nanoparticle catalyst. J Electroanal Chem, 2008, 614: 93–100
53 Moniri S, Van Cleve T, Linic S. Pitfalls and best practices in measurements of the electrochemical surface area of platinum-based nanostructured electro-catalysts. J Catal, 2017, 345: 1–10
54 van der Vliet D F, Wang C, Li D, et al. Unique electrochemical adsorption properties of Pt-skin surfaces. Angew Chem Int Edit, 2012, 51: 3139–3142
55 Alcaide F, Alvarez G, Cabot P L, et al. Supporting PtRh alloy nanoparticle catalysts by electrodeposition on carbon paper for the ethanol electrooxidation in acidic medium. J Electroanal Chem, 2020, 861: 113960
56 Chen D, Tao Q, Liao L W, et al. Determining the active surface area for various platinum electrodes. Electrocatalysis, 2011, 2: 207–219
57 Durst J, Simon C, Hasché F, et al. Hydrogen oxidation and evolution reaction kinetics on carbon supported Pt, Ir, Rh, and Pd electrocatalysts in acidic media. J Electrochem Soc, 2015, 162: F190–F203
58 Ianniello R, Schmidt V M, Stimming U, et al. CO adsorption and oxidation on Pt and Pt-Ru alloys: Dependence on substrate composition. Electrochim Acta, 1994, 39: 1863–1869
59 Green C L, Kucernak A. Determination of the platinum and ruthenium surface areas in platinum-ruthenium alloy electrocatalysts by underpotential deposition of copper. I. Unsupported catalysts. J Phys Chem B, 2002, 106: 1036–1047
60 Mayrhofer K J J, Strmcnik D, Blizanac B B, et al. Measurement of oxygen reduction activities via the rotating disc electrode method: From Pt model surfaces to carbon-supported high surface area catalysts. Electrochim Acta, 2008, 53: 3181–3188
61 Garrick T R, Moylan T E, Carpenter M K, et al. Electrochemically active surface area measurement of aged Pt alloy catalysts in PEM fuel cells by CO stripping. J Electrochem Soc, 2017, 164: F55–F59
62 Oviedo O A, Vélez P, Macagno V A, et al. Underpotential deposition: From planar surfaces to nanoparticles. Surf Sci, 2015, 631: 23–34
63 Fiçicioğlu F, Kadirgan F. Characterization of a Pt + Pd alloy electrode by underpotential deposition of copper. J Electroanal Chem, 1993, 346: 187–196
64 Shao M, Odell J H, Choi S I, et al. Electrochemical surface area measurements of platinum- and palladium-based nanoparticles. Electrochem Commun, 2013, 31: 46–48
65 Lohmann-Richters F P, Abel B, Varga Á. *In situ* determination of the electrochemically active platinum surface area: Key to improvement of solid acid fuel cells. J Mater Chem A, 2018, 6: 2700–2707
66 Tritsaris G A, Nørskov J K, Rossmeisl J. Trends in oxygen reduction and methanol activation on transition metal chalcogenides. Electrochim Acta, 2011, 56: 9783–9788

Summary for “Pt合金催化剂电化学活性面积表征方法综述”

Review on electrochemical active surface area characterization methods of Pt alloy catalysts

Hui Zhang[1], Fen Zhou[1,2] & Mu Pan[1,2*]

[1] *State Key Laboratory of Advanced Technology for Materials Synthesis and Processing, Wuhan University of Technology, Wuhan 430070, China;*
[2] *Foshan Xianhu Laboratory of the Advanced Energy Science and Technology Guangdong Laboratory, Foshan 528200, China*
* Corresponding author, E-mail: panmu@whut.edu.cn

Proton exchange membrane fuel cells (PEMFCs) are one of the most promising technologies for clean energy. However, some fundamental challenges remain to be addressed before PEMFCs with low Pt usage become the top contender. To achieve high-performance and cost-effective in PEMFCs, Pt-alloy catalysts are currently one of the bright catalyst candidates. Electrochemical active surface area (ECSA) is a key indicator to gauge the performance of Pt catalysts and an important parameter in studying catalytic kinetic issues in PEMFCs. Therefore, the accurate estimation on the ECSA is exceptionally critical. Known and mature ECSA characterization methods for Pt/C catalysts have been established, which have been widely available for many decades. However, there are issues remaining for ECSA characterization of Pt-alloy catalysts due to the significant difference in properties, such as composition, particle size, shape compared with Pt catalysts. Therefore, the ECSA characterization approaches for Pt/C catalysts cannot be transplanted to Pt-alloy catalysts since the characterization accuracy will no longer meet the requirement.

In this review, the present characterization methods of ECSA for Pt-alloy catalysts and their inaccuracy sources are described and explained, including physical methods and electrochemical methods. The physical methods cover X-ray diffraction (XRD) and transmission electron microscopy (TEM), while hydrogen underpotential deposition (H-upd), carbon monoxide stripping (CO-stripping) and underpotential deposition of metals are classified as electrochemical methods. The ECSA obtained from XRD and TEM is considered to be theoretical ECSA to evaluate the catalyst utilization. Therefore, the ECSA calculated from XRD and TEM is usually used as a reference. Owing to the differences in surface adsorption properties after alloying, it will be underestimated the ECSA of Pt-alloy catalysts by H-upd and CO-stripping, which lead to exaggerate specific activity compared with Pt/C catalysts. Generally, it is accepted that the surface area from electrochemical methods is active, but in fact it is still controversial. The surface area of different metal components of Pt-alloy catalysts could be quantified by metal underpotential deposition method. Since the contribution of different metal components to the catalytic activity is different, the actual ECSA cannot be simply calculated by adding the respective metal surface area.

The active surface area of Pt-alloy catalysts is affected by many factors, making it hard to develop a universal method to characterize the ECSA accurately. To evaluate the performance of Pt-alloy catalysts more objectively, it is necessary to clarify the relationship between the surface structure of Pt-alloys catalysts and adsorption energy as well as the coverage of adsorbed species. It is essential to develop an innovative electrochemical method with high accuracy which is also important and urgent for the research on new Pt-alloy catalysts with high-performance.

proton exchange membrane fuel cells, Pt alloy catalysts, electrochemical active surface area, physical characterization, electrochemical characterization

doi: 10.1360/TB-2022-0795